Environ Model Assess (2009) 14:29–45
DOI 10.1007/s10666-008-9164-4

Mechanistic Virtual Modeling: Coupling a Plant Simulation Model with a Three-dimensional Plant Architecture Component

Eric Jallas · Ron Sequeira · Pierre Martin · Sam Turner · Petraq Papajorgji

Received: 9 October 2006 / Accepted: 23 June 2008 / Published online: 30 September 2008

Abstract The aim of this research is to integrate plant architectural modeling or "visualization modeling" and "mechanistic" or physiologically based modeling to describe how a real plant functions using a virtual crop. Virtual crops are life-like computer representations of crops based on individual plants and including the representation of the substrate on which the plants grow. The integration of a three-dimensional expression and the mechanistic model of plant development and growth requires the knowledge of the position of the organs along the different plant axes (the topology), their sizes, their forms, and their spatial orientation. The plant simulation model simulates the topology and organ weight or length. The superposition of spatial position and the topology produces the architecture of the plant. The association between sizes and organs creates what we refer to as the plant morphological model. Both components, the architectural model and the morphology model, are detailed in this paper. Once the integration is complete, the system produces a movie-like animation that shows the plant growing. The integrated model may simulate one or several plants growing simultaneously (in parallel). Visual capabilities make the proposed system very unique as it allows users to judge the results of the simulation the same way a farmer judges the situation of the crops in real life, by visually observing the field.

Keywords Crop modeling · Virtual simulation · Cotton · Virtual plant

E. Jallas · P. Martin
CIRAD,
TA 179/04, Avenue Agropolis,
34398 Montpellier, Cedex 5, France

E. Jallas (✉)
ITK,
5 rue de la Cavalerie,
34000 Montpellier, France
e-mail: jallas@cirad.fr
URL: www.itkweb.com

S. Turner
1779 Wade Road,
Starkville, MS 39759, USA

R. Sequeira
USDA–APHIS–CPHST,
1017 Main Campus Drive, Suite 2500,
Raleigh, NC 27606, USA

P. Papajorgji
IFAS, Information Technologies Office, University of Florida,
Gainesville, FL 32611, USA

1 Introduction

Plant architectural modeling or "virtual" or "visualization" modeling proposes to recreate visually realistic, three-dimensional plants based on field sampling and the application of an algorithm to standardize the three-dimensional description of a plant. "L-systems" [26] and the "Reference Axis" [11] are two of such approaches. Mechanistic or physiologically based modeling proposes to describe how a plant functions. This approach recreates physiologically realistic plants based on estimates of physiological development and growth status. These estimates are derived from mathematical expressions of the interactions between plant components that are in turn derived from field experimentation and all of which are integrated into the simulation model proper. Our objective is to integrate both modeling

paradigms. The approach we developed was initially based on the "mechanistic" approach but asks the question: what functionality is inherent in the three-dimensional architecture of the plant and how can this functionality be integrated into a unified "Virtual Plant" model? The subsequent question is, how does this integrated system allow us not only to enrich the overall representativity of the model (in the sense that there is a better correspondence with perceived reality) but also to enhance the usefulness of the system for producers and managers? We used functions and concepts obtained from mechanistic and architectural modeling theories and created an integrated system. The system is developed by enhancing a base "mechanistic" model, GOSSYM [4], with three-dimensional architectural component. We accomplished this by associating actual locations in three-dimensional space to growth and development functions.

2 Crop and Crop Architectural Models

Crop modeling started at the end of the 1960s and beginning of the 1970s [7, 18] based on previous plant process modeling [16, 17] and ecosystem simulation work [38]. Later and parallel to crop modeling efforts elsewhere, a "plant architectural modeling" approach was initiated [11, 19]. Both disciplines grew independently. Crop modeling focused on a more mechanistic description of growth and development processes, whereas plant architectural modeling focused on better comprehension of morphogenetic rules in addition to providing a better representation of plant architecture. The goal of crop modelers to deliver a decision tool useful at the farm level led them to develop their models on the desktop or personal computer. This constraint was not compatible with the goal of the plant architecture modelers. In order to produce better and more realistic images, they needed larger, more powerful computers with extended graphical capacities. At the time, the hardware required by the graphical imaging included in the architectural modeling effort was almost two times faster than the systems in use by most mechanistic modelers. Furthermore, due to the basic incompatibilities of the development environments used by architectural and mechanistic modelers, the integration of physiological mechanistic realism and morphological architectural visual realism was not possible.

Currently, the level of the biological complexity included in computerized crop models is very high. This assessment is based on the fact that existent models include all physiological responses that are relevant to production and crop management. Models like GOSSYM can simulate canopy light interception and net photosynthesis, individual leaf, internode, and fruit growth, spatial root growth, etc. However, crop models are currently not common farming tools. Cox [9] suggested that this lack of technology transfer could be inherent in the crop models themselves. They are developed by scientists to integrate their knowledge, not by communication specialists to solve production problems. Furthermore, crop models require numerous types of information that could be difficult to obtain by a farmer (e.g., daily solar radiation) or which could seem without direct relevance to the farmer. (e.g., soil desorption curve).

Architectural models and associated visualization tools are so realistic that they are used in the film [15] and computer gaming industries. Increases in computer power and graphics capabilities have made high-performance graphics packages available on desktop systems. Plant architectural modelers seem to have attained their goal and are starting to consider integration of their models with crop physiological models [34].

Today, acquiring data with automated sensors and remote transfer is no longer an insurmountable problem and is increasingly possible around the world. The level of knowledge integrated in a crop model is sufficient to produce decision support systems able to answer key management questions from producers. Thus, the criticism voiced by Cox [9] is not entirely justified. Perhaps, the main problem resides in the interface of the crop model with the farmer [37]. Crop models produce numbers and graphs, but the farmer deals daily with a three-dimensional world. What can an average plant dry weight of 125 or of 150 g mean to a farmer? However, if this difference was expressed as an image of two different plants, the farmer would immediately understand and even propose a technical action to remedy the problem. The same can be said about expressing nitrogen status as a nitrogen rate or as a picture of a chlorotic plant. Given that today personal computers are able to simulate 3D virtual plants, it is reasonable to propose associating a graphical interface with crop models. The effort is certainly justifiable in terms of increased usability of the model and in terms of its use as a surrogate for experimentation. Furthermore, we believe that there is intrinsic functionality in the three-dimensional structure of a plant, which is expressed as part of the plant's response to its environment. This functionality will include aspects such as the density of the aboveground "tubing" (the physical characteristics of xylem vs. phloem bundles) that will affect plant water potentials and nutrient transport. The architectural dynamics will change depending on management-relevant factors such as loss of apical dominance due to insect/hail damage. Therefore, we believe that the inclusion of this three-dimensional architecture with its attendant physiological interactions will improve our management capabilities and the robustness of our overall system.

3 Materials and Methods

In order to simulate a plant in three dimensions, we need to be able to simulate the following characteristics:

- The topology of the plant. Topology describes organ organization along the plant axes. This organ organization specifies for each organ, its type (internode, bud, leaf, etc.), what organ bears it, and what organs it is bearing. For the aboveground plant parts, the different organs identified are internodes (on monopodial or sympodial nodal units), leaves (cotyledons, fruiting, or mainstem leaves), and fruit (squares, flowers, green bolls, and open bolls).
- The sizes of each organ, its length, diameter and width. This is the morphology of each organ, and this morphology is the result of the growth process.
- The spatial position and the shape of each organ. This corresponds to the plant geometry.

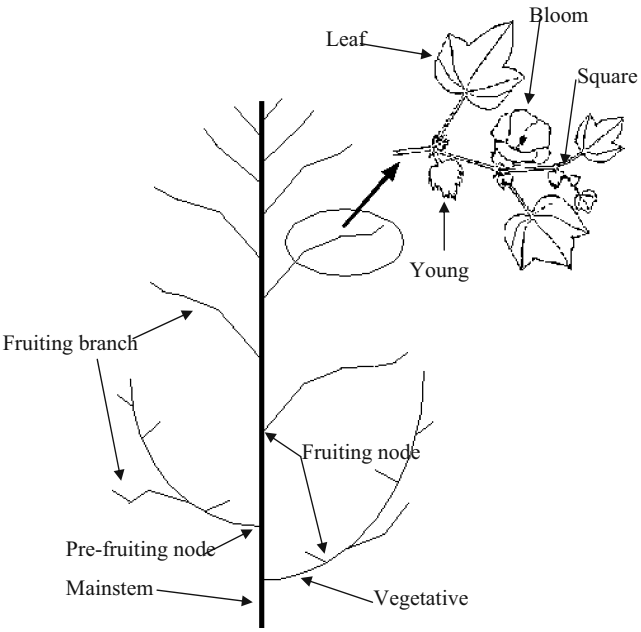

Fig. 1 Aboveground organs individualized in GOSSYM

4 Description of the Output of the GOSSYM Cotton Plant Model

4.1 Topology

The original GOSSYM model simulates the topology of an "average" cotton plant [4]. In 1998, Jallas [24] modified the light interception model of the original GOSSYM model, added stochasticity in the topology submodel, and added the architectural and 3D simulation engine described in this paper. However, even if stochasticity has been added to different processes, the biological functions described in this part of the paper are the same as the original GOSSYM.

The plant topology is the result of morphogenesis, which includes two subsequent processes which are the differentiation of the organ (or its initiation) and the organ evolution. Morphological events are estimated from the age of each bearer organ in relation to an age threshold. The threshold age is a function of environmental variables interacting with varietal behaviors. Three main factors drive morphogenesis: temperature, water, and nitrogen availability and carbohydrate supply.

In the morphogenesis model, GOSSYM makes a distinction between the following aboveground organs Fig. 1:

- The mainstem bearing the prefruiting nodes and the fruit-bearing nodes. Prefruiting nodes may develop into vegetative branches. Fruit-bearing nodes always develop into fruiting branches as growth proceeds
- The vegetative branches, which also have fruit-bearing nodes which in turn develop into fruiting branches
- Fruit-bearing nodes bearing the "squares" (floral buds). These squares develop into flowers and then bolls (the fruit), consisting of a carpel, seeds, and fiber. Flower buds, flowers, and bolls may abort at a young stage
- Finally, GOSSYM considers that there is a leaf at the axil of each node; the first two leaves are cotyledons

4.2 Organogenesis

Temperature "experienced" by the plant organ being considered has a direct effect on morphogenesis. This effect is not linear, so GOSSYM [4] does not use sums of temperatures (GOSSYM makes no distinction between plastochron and phyllochron). The temperature "experienced" is used in (usually) quadratic polynomial equations (see equation for *Minimum_Time* in Eq. 1) to determine the age thresholds at which the various organs should be initiated or differentiate.

For all the creation events, the time interval between them is determined by the following generic equation [22]:

$$\begin{aligned} &\text{If} \quad : \text{Age} \geq \text{Minimum\_Time} + \sum \text{Delay(i)} \\ &\text{Then} \ : \text{Create an} \quad \text{organ (x) today} \end{aligned} \tag{1}$$

where:

Minimum_Time	$(a + b \times T + c \times T^2) \text{x} C$
Age	the actual age of the last event of reference
Delay (i)	the delay induced by factor i, which can be a water stress, a nitrogen stress, or a carbohydrate stress,

T	the average temperature "experienced" by the last event of reference,
C	a varietal calibration factor,
a, b, and c	three local parameters.

Stresses experienced by the plant modify growth and development (they are the "Delays" in Eq. 1). Their effect can be direct or indirect. For example, as direct effects, small water stresses will accelerate morphogenesis by changing the "level" of the first fruiting branch. Equation 2 shows this direct effect: If the plant experiences numerous water stresses, then the number of days necessary between emergence and first square will be reduced, and the plant will start its reroductive stage earlier.

$$\begin{aligned} &\text{If} \quad : \text{D.A.E.} \geq \text{Minimum\_Time} - \sum \text{Water\_stress}(i) \\ &\text{Then} \ : \text{Create the first fruiting branch today} \end{aligned} \tag{2}$$

where:

Minimum_Time	$(a+b\times T+c\times T^2)\times C$,
D.A.E.	is the number of days after emergence,
Water_Stress (i)	a level index of the water stress for the day i (between 0 and 1),
T	the average temperature "experienced" by the last event of reference,
C	a varietal calibration factor,
a, b, and c	three local parameters.

But, at the same time, if these water stresses are severe, then they can also induce carbohydrate or nitrogen stresses by reducing net photosynthesis or nitrogen uptake. In this case, a water stress will, as an indirect effect, slow down morphogenesis (Eq. 1). Nitrogen stress and carbohydrate stresses always slow down or even stop morphogenesis. These stresses are calculated prior to the calculation of growth and development [4].

4.3 Morphogenetic Differentiation

The various morphological phases can be separated into four: creation of organs, organ evolution, changes in phenological stage, and abscission. The sequence of organ creation is as follows:

- First, there is the appearance of prefruiting nodes on the mainstem; then, if temperature permitting, the first fruiting branch with the first flower bud (square) appears
- Once the first fruiting branch has formed and if temperature and nutrient conditions are appropriate:
  - ✓ Prefruiting nodes on the mainstem develop into a vegetative branch, and further, fruiting branches appear on the main branch and on formed vegetative branches
  - ✓ Appearance of squares and nodes on fruiting branches of both the mainstem and vegetative branches

The sequence of fruit organ evolution is the following: transition of square to flower, then to abscisable (i.e., susceptible to premature dehiscence boll), then into a non-abscisable capsule (green boll), and finally maturation of the capsule (open boll). For these organ evolution events, the time interval between them is determined by the following generic equation [22]:

$$\begin{aligned} &\text{If} \quad : \text{Age}_{\text{stage(i)}} \geq \text{Minimum\_Time} \\ &\text{Then} \ : \text{Change from stage } i \text{ to stage } i+1 \\ &\text{(Stages are square, bloom, young boll, green boll and open boll).} \end{aligned} \tag{3}$$

where:

Minimum_Time	$(a+b\times T+c\times T^2+d\times F(\alpha)+e\times F(\alpha)^2+f\times F(\alpha)T+g\times F(\alpha)T^2)\times C$
$\text{Age}_{\text{stage}(i)}$	the actual age, in the stage (i), of the considered organ,
T	the average temperature experienced by the organ,
$F(\alpha)$	the application rate of the factor α which can be a growth regulator or a defoliant,
C	a varietal calibration factor,
a, b, c, d, e, f, and g	seven local parameters.

4.4 Abscission

The rules for organ abscission are relatively simple. Two principles are used:

- Leaf shedding is caused by senescence. In turn, senescence may be due to natural ("age rule") or to the use of defoliants ("defoliant rule").
- Fruit shedding is governed by nutritional theory. The nutritional theory hypothesizes that fruit number is correlated with the plant carrying capacity. In the case of the cotton plant, this postulates that fruit initiation and abscission depends on the supply–demand ratio in carbohydrates [21].

The "age rule" for leaves leads to the following: The leaf is shed if it is older than a given age threshold (90 days—5

leaf area index [LAI]) and if the LAI is greater than 3 [23]. Translation of the "defoliant rule" is more complex. First, the model calculates the number of leaves that will be shed naturally this day because of their age. Second, the model calculates a theoretical total number of leaves to be shed by defoliant application on the day in question. This number is equal to the number of remaining leaves the day before the defoliant application multiplied by a shedding factor. Third, the model calculates the difference between the theoretical number of leaves to be shed by defoliation and the number of leaves which will shed for age reason. This difference is the number of leaves that must be shed due of use of defoliant. GOSSYM thus sheds the required number of leaves, starting with the oldest. The shedding factor, expressed as a proportion of total leaves that will be abscised (0–100%), is:

$$\text{Fabs} = \left(a + b \times \overline{T} + c \times \text{Def} + d \times \text{Dt} - e \times \psi - f \times \psi^2 + g \times \overline{T} \times \text{Def} \times \text{Dt} \times \psi\right) \times C \quad (4)$$

where:

$\overline{T}$	the average temperature "experienced" by the organ,
Def	the leaf defoliant concentration,
Dt	the period of time since the defoliant application,
ψ	the leaf water potential,
C	a varietal calibration factor,
a, b, c, d, e, f, and g	seven local parameters.

Because GOSSYM simulates an average plant, the abscission submodel calculates the proportion fruits that should be abscised at each specific fruit location (the position of the fruit in the simulated plant topology). This is calculated for all the fruits location with an abscisable fruit. Then, abscission of fruits is expressed as a reduction in the proportion (with values in [0–1]) of fruits at the location in question and is determined in two stages. The model calculates the daily theoretical losses of fruits (Floss) then compares these theoretical losses with the number of squares (2 to 30 days old) and capsules (bolls) which can still be shed (up to 21 days old). Shedding is done as follows according to the following comparisons:

- If there are sufficient organs of each type, they are shed (percent of reduction) in their respective proportions up to a maximum of 50% of squares and 30% of young bolls (e.g., three squares should be shed today, and there are 12 squares on the plant, so at each square location, 3 of 12 [here equivalent as 25%] of the square will be "removed").
- If there are not enough organs of each type which the model has calculated that need to be shed, another organ type is shed to compensate, up to a maximum of 30% for the young capsules (bolls).
- The number of organs shed cannot exceed the number sheddable as determined by the fixed shed thresholds.
- Finally, one fruit is totally shed at a specific location when the proportion of the fruit at this location is below 0.001.

The theoretical fruit loss equation is as follows:

$$\text{Floss} = C - 3.60717 \times F_{\text{stress}} + 1.6047 \times (F_{\text{stress}})^2 \quad (5)$$

where:

Floss	calculated daily fruit loss in number of fruits [0–3],
F_{stress}	the "combined" stress factor for fruit organs,
C	a varietal calibration parameter that changes according to the green capsule (boll) weight/plant weight ratio.

4.5 Organ Growth and Weight

As is true for the topology, GOSSYM also simulates organ sizes. The philosophy followed in GOSSYM is in the lineage of work of [16, 17]. The modeling of growth in GOSSYM is based on the idea that "crops have a growth potential when there are no limiting factors such as availability of carbon, nitrogen or water" [36]. This modeling approach calculates daily the following factors:

- The growth in mass of the stems and the pool of roots
- The growth in mass of each individual leaf and fruit
- The growth in area of the various leaf categories (leaves at prefruiting nodes, leaves at fruiting branch nodes, leaves at fruit-bearing bud nodes) and the LAI
- The increase in length of the various internodes and the vertical growth of the plant
- The carbohydrate available for the next day and excess carbon that is unusable for growth

The procedure is as follows:

First, the model calculates the water status of the plant and estimates three different water stress reduction factors

(all are noted in the paper as F_{H2O} and their values range between [0, 1]). One is for the leaves, another for the stems, and the third for other plant parts. The variables used to calculate these water stresses are soil and leaf water potential, average temperature, and incident radiation. For example (only one water stress factor equations is described here; the others have a similar form), the equation for the water stress of affecting other plant parts than leaf and stem is:

$$F_{H2O} = \frac{a}{\psi_{soil} + b} + c \times \overline{T} \times \psi_{soil} + d \times I_R \quad (6)$$

where:

$\overline{T}$	the average temperature "experienced" by the plant,
ψ_{soil}	the average soil water potential for the root zone,
I_R	the incident radiation,
a, b, c, and d	four parameters.

Then, the model estimates potential growths (in grams of dry matter) for the aboveground portions of the plant. This is done organ by organ according to the weight and/or area of each organ, the temperature, and age [2–4, 23]. Organ definition is a little different for growth than for topology. Internodes are not considered individually but as a pool forming a stem. GOSSYM simulates the growth of the stem and does not simulate the growth of each internode. This choice has some implications to the simulation of the size of each organ identified at the topological level. The potentials of growth are reduced according to the water status of the plant and the use of growth regulators. Organ potentials are totaled as overall growth potential by type of organ [25, 27]. For potential growth, the generic equation is:

$$\begin{aligned} \text{Potential\_Growth}_{\text{Organ}(i)} = \text{Biomass}_{\text{Organ}(i)} & \\ \times \left(a + b \times \overline{T} + c \times \overline{T}^2\right) & \\ \times \left(\prod R(f)\right) \times \text{Dt} \times C & \end{aligned} \quad (7)$$

where:

$\text{Biomass}_{\text{Organ}(i)}$	the actual biomass of the organ (i), expressed in weight (g) or area (cm^2),
T	the average temperature "experienced" by the organ,
$R(f)$	a reduction coefficient linked to the factor f,
Dt	the period of time,
C	a varietal calibration factor,
a, b, and c	three local parameters.

In the second set of operations, root growth potential (in grams of dry matter) is assessed. For this calculation, at the start of growth, root weights are preset at 0.005 to 0.035 g per cell in a few soil cells. The model then calculates the vegetative mass distribution ratio (root weight/weight of leaves and branches). The ratio is compared with a theoretical value (according to the weights of leaves and branches and plant water status), and the growth potentials per type of organ calculated in the first phase are adjusted [6].

The equation is:

$$\begin{aligned} \text{Root\_mass} = & \left(a + b \times e^{c(\text{Leaves\_weight}+\text{Stem\_weight})}\right) \\ & \times (d - g \times F_{H2O}) \times C \end{aligned} \quad (8)$$

where:

F_{H2O}	the water stress factor,
C	a varietal calibration factor,
a, b, c, d, and g	five local parameters.

In the next step, GOSSYM uses these adjusted growth potentials to calculate the demand for carbohydrate and compares it with its supply which is the sum of net photosynthesis per day and the available pool of carbohydrate. The carbohydrate "supply/demand" ratio (from 0 if supply is nil to 1 if supply is greater than demand), "representing carbon stress" is then used for fresh adjustment of growth potentials by plant organ type.

The model then uses adjusted growth potentials to calculate nitrogen requirements and determines three nitrogen stress ratios for the fruits (whose demand is met as a priority), for the aboveground components and for the roots. GOSSYM uses these ratios to calculate three combined carbon/nitrogen stress ratios. These make it possible to calculate effective growth in weight and area of the various organs on an individual basis. The effective growth of an organ is the product of the multiplication of its individual growth potential by the combined stress ratio for the type of organ.

Finally, the model calculates elongation (in cm) of the mainstem. Three distinct periods are considered for this: (1) a solely vegetative phase (before the appearance of the first fruiting branch), (2) a phase during which the first two fruiting branches appear, and finally (3) the third phase concerning subsequent plant growth. Daily growth is calculated from the age of the last node or the last three nodes, according to the phase, and is reduced by water stress [8], by applications of PIX^R (mepiquat chloride [1, 1-dimethyl-piperididinium chloride], a growth regulator) and of defoliants. The generic equation for elongation is:

$$\begin{aligned} \text{Elongation} = & \left(a + b \times \overline{\text{Age}} + c \times \overline{\text{Age}}^2\right) \times F_{H2O} \\ & \times F_{PIX} \times F_{PGR} \times C \end{aligned} \quad (9)$$

where:

$\overline{\text{Age}}$	the average age of the last nodes (maximum the last 3),
F_{H2O}	the water stress reduction factor,
F_{PIX}	the PIX reduction factor,
F_{PGR}	the growth regular reduction factor,
C	a varietal calibration factor,
a, b, and c	three local parameters.

4.6 Description of Field Data Sets Collected to Validate the New Model

GOSSYM simulates the topology of the plant and the growth of each organ. In order to simulate a virtual plant, we need also to be able to translate weight and length of each organ into their "visual sizes" and to position each organ in the 3D space. This information was obtained using data from two experiments. The first experiment was a field experiment conducted at Montpellier, France, in 1994. The second experiment was conducted at Mississippi State University's North Farm at the US Department of Agriculture–Agricultural Research Service–Crop Simulation Research Unit facilities, Starkville, MS (hereafter referred to as Mississippi State experiment) using growth chambers known as Soil–Plant–Atmospheric-Research (SPAR) units [29].

4.7 Montpellier Experiment

The field experiment was conducted at «Domaine de La Valette» in France. Four factors were tested in a Criss-cross design [30]. The field was plowed at the end of April and sown May 6 with a plant density of 48,000 plants per hectare. Emergence was observed May 15. Fertilized plots received 20 units of N in four applications, and all plots received three applications of 750 g of Bore per hectare. Irrigated plots received three irrigation applications for a total amount of 357 mm of water. The field had herbicide applied April 26 with Treflan, insect management concerned *Thrips* at the beginning of June, and *Heliotis* at the beginning of September. A crop maturation defoliant (PREP) was applied in September/October at the rate of 2L/ha. Plots were harvested in October for Pavlikéni and in November for DES 119 cotton varieties.

Observations were continuous from planting to harvest. Nondestructive weekly observations included emergence rate, plant height, plant mapping, and phenological stages. In addition to these periodic nondestructive measurements, 30 green bolls were harvested mid-September on four of the blocs (120 bolls) and 50 leaves per cultivar on different plants and at different positions (randomly). The diameter of each boll was measured, and the bolls were dried at 60°C to constant weight to determine dry matter accumulation. Petiole length, leaf length, and leaf area were measured with a scanner.

4.8 Mississippi State University Experiment

The experiment was conducted in growth chambers (SPAR units). These units are used for controlled environment experiments and they have been described by Acock et al. [1] and Reddy et al. [32, 33]. These units use natural lighting and have the capability to control ambient air temperature, vapor pressure deficit, and CO_2 concentration at predetermined set points for studies of plant growth in natural solar radiation regimes. A dedicated computer controls air temperature, CO_2 concentration, and soil watering in the SPAR units. The computer conducts continuous monitoring of all important response variables as environmental variables and plant gas exchanges. The temperature in each SPAR unit is monitored and adjusted every 10 s throughout the day and night. The temperature is maintained within ±0.5°C of treatment set points. The CO_2 concentration in each SPAR unit is monitored every 10 s and integrated over 900-s intervals throughout the day and night. The CO_2 concentration is maintained within ±10 μL L^{-1} of set point (350 μL L^{-1}). Dew point temperature, global radiation, and quantum flux of photosynthetically active radiation are collected every 10 s and integrated over 900-s intervals.

Nine units were used for this experiment: Three were set at 20/12°C (day/night temperature – cold), two other units were set at 25/17°C (low temperature), two units at 30/22°C (medium temperature), and two units at 35/27°C (high temperature). The units were planted on April 21, with Deltapine DP5415BT cotton seeds, in pots made of polyvinyl chloride pipe (0.15 m diameter, 0.67 m length) with a volume of 12 L. The growing medium was sand. Four cotton seeds were planted in each pot placed in the SPAR units. SPAR units for cold, low, and medium temperature received 18 pots, and SPAR units for high temperature received 24 pots. Pots were arranged to obtain a regular plant population equivalent to 18 plants per square meter when plants will enter into competition for light. Plants were thinned to a single plant at postemergence. Three times a day, a complete Hoagland's nutrient solution was delivered to each row or pot of plants via a drip irrigation system.

Observations were continuous from planting date to the end of the experiment, which was 2 month after the planting date. Nondestructive daily observations included emergence rate, internode lengths, and mainstem leaf lengths on six plants in each growth chamber; timing of mainstem node formation was observed on the same six plants per units. In

addition to these periodic nondestructive measurements, three harvests of six plants (six pots) per unit harvested were performed at three different phenological stages as follows: two true leaves, four true leaves, and squaring. At each of these three harvests, the plants were dissected into leaves, nodes, roots, and squares (if any). Plant leaf areas, petiole length, and plant heights were measured. All the plant components were dried at 75°C to constant weight to determine dry matter accumulation.

4.9 Integration of the Mechanistic and Architectural Models

Figure 2 shows the main components of the system and their relationships [28]. The system is controlled by a component referred to as SimulationController that receives the input data related to field conditions, technical itinerary, and weather information and runs the simulation for a day. The SimulationController asks the CottonSimulator (the GOSSYM model) to calculate the daily values that are used by the PlantArchitecture component to simulate plant architecture and places the results in a three-dimensional matrix. Then, the DisplayComponent is activated to display on the screen the results of the simulation for the current day.

Specifically, the original mechanistic model simulates daily cotton growth, which includes daily plant topology (i.e., relative position between organs) and organ weight or length. The new morphological component simulates the morphology of the plant, which includes organ forms and sizes. The architecture component simulates the 3D geometry of the cotton plant. This includes insertion angles, bending of branches, and diameter transition.

The DisplayComponent were developed with OpenGL™ functions. The output of the architectural submodel is a three-dimensional matrix that OpenGL functions project on the two-dimensional space of the screen. There are more than 150 functions in OpenGL [20], and these functions allow the user to manage scene lighting, shading, object texture, color, three-dimensional depth, and perspective effects among others.

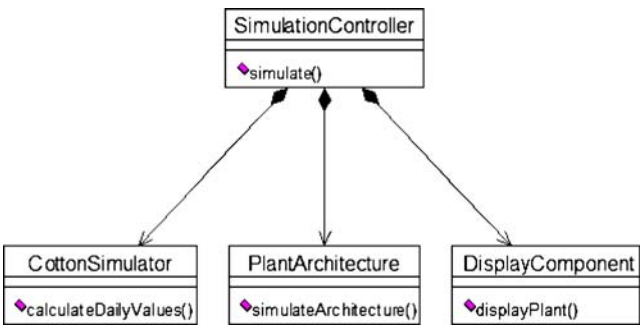

Fig. 2 Integration of GOSSYM, the architectural engine, and display components

5 Results and Discussion

A plant can be described as a unique topological and geometrical assembly of *n* organs of different size and age. The visual perception of a plant is then the three-dimensional expression of its topology and geometry. As discussed before, the ability to visualize simulations of plants provides intuitive insight into its topology, geometry, and most importantly, the physiological implications of those features either in terms of potential or in term of constraints. For example, Room et al. [34] proposed to use their visual model to test, in a "virtual experiment," the best petiole length for the highest light interception efficiency. To be able to calculate this efficiency, we need to be able to calculate "gains" and "losses" or costs. With a "visual model," it is easy to calculate the best petiole length for light interception at any given time, but it is impossible to calculate the real cost, over the growing season, of this best petiole length. The reason is that part of the plant production "costs" are linked to physiological processes, which evidently do not have any direct visual expression, such as light respiration, maintenance respiration, and transpiration. Crop models can calculate these physiological costs, and of course, these models lack plant architectural and geometrical information. The kind of expanded functionality not heretofore present in a single system was developed and is described in these results.

As discussed above, to simulate a virtual plant, we need to know the organization of the organs along its different axes (the topology), their sizes, their forms, and their spatial orientation. GOSSYM simulates the topology and their weight or length. The superposition of spatial position and the topology is the architecture of the plant. Association between sizes and organ forms could be called the plant morphological model. Both processes, the architectural model and the morphology model, are described as follows.

6 Simulation of the Architecture (Positioning and Morphology)

The "architecture" specifies geometric relationships between subsequent organs, the assembly of which gives the specific shape of each plant. To simulate this architecture on a computer, a graphical symbol (a shape) and a coordinate system specification must correspond to each organ. The graphical symbol is built with a given number of polygons, for example three polygons for an internode and 14 polygons for a leaf (see Fig. 3). The coordinate system corresponds both to a rectangular coordinate system associated with the graphical symbols and to a spherical coordinate system associated with the geometrical position of the organ.

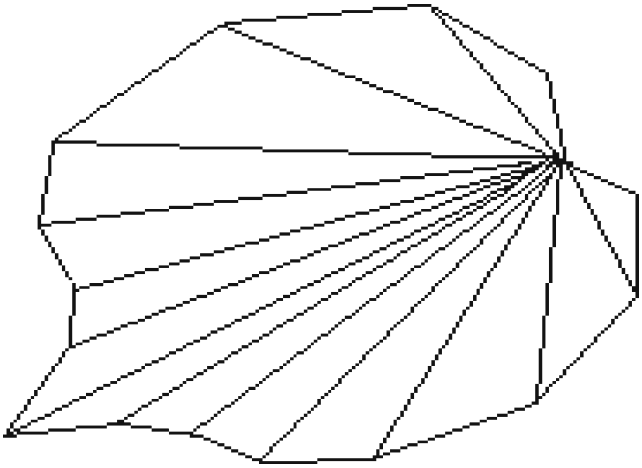

Fig. 3 Leaf symbol used by the visualization system is composed of 14 polygons

The length, diameter, and thickness of each organ correspond to the normal of the different vectors describing the rectangular coordinates (see Fig. 4). The spatial position of the origin of the system, the direction of the organ minimum inertia axes, and the two angles of direction in planes defining the vector space define the geometrical position of an organ.

The PlantArchitecture component integrated with the GOSSYM model simulates architectural characteristics and places the rectangular coordinates spatially. Key architectural characteristics are phyllotaxy, insertion angles, and shapes.

Positioning the rectangular coordinates in space supposes knowing the origin and two directions, and the third one is inferred. One of these directions is called the main direction, and the other one is called the secondary direction. By definition, the origin is always at the extremity of the previous organ called the "porter." The main direction is determined from the insertion angle of the organ with the main direction of the porter. The secondary direction is determined by the rotation angle in the main plane defining the vector space.

6.1 Internode Positioning

Internode position is determined with insertion angles and axis angles. The insertion angle is the angle between the porter and the internode. The first internode is a special case because there is no porter. Thus, the insertion angle of the first internode is determined in relation to the vertical direction and it value is 0°. All other mainstem internodes also have an insertion angle of 0°. The axis angle gives the secondary direction. After positioning the internode, the system applies the phyllotaxy on each internode of the main axis. By definition, the phyllotaxy determines the axis angle of the first internode of the branch barred by the mainstem internode. This phyllotaxy is, for cotton, a counterclockwise rotation of 135° (3/8 phyllotaxy or $3/4\pi$). The insertion angle of the first internode of the fruiting branch is variety dependent. In our data, insertion angles (θ_0) were from 50° to 70° (see Fig. 5a). As shown on Fig. 5a, on each fruiting branch, internodes younger than the first have a higher insertion angle except for the last which tends to be redressed. For most of the commercial cotton cultivars, fruiting branch bending is characterized by this flexion toward the ground in the first part of the branch and a reverse flexion up at the end of the branch. This bending is certainly linked to the branch weight. The architectural simulation must reproduce it. Our model for this bending was developed by de Reffye [10–12, 14], and it uses concepts from material resistance theory [5]. It can be demonstrated (see Appendix) that for a small flexion, when a force F is applied at a determined position of a branch (see Fig. 15 in Appendix), the flexion angle of the branch (w) could be approximated with the following relation:

$$w = \frac{\sin\theta_0\left(1 - \cos\left(\sqrt{\cos\theta_0} \times K \times h\right)\right)}{\cos\theta_0 \times \cos\left(\sqrt{\cos\theta_0} \times K \times h\right)} \tag{10}$$

where:

K	$\sqrt{\frac{F}{E \times I}}$,
E	the elasticity modulus or "Young" modulus,
I	$\frac{\pi \times R^4}{4}$, in the case of a bar with circular section where R is the radius of the section,
h	the distance between branch insertion and point of force application,
θ_0	the insertion angle of the branch.

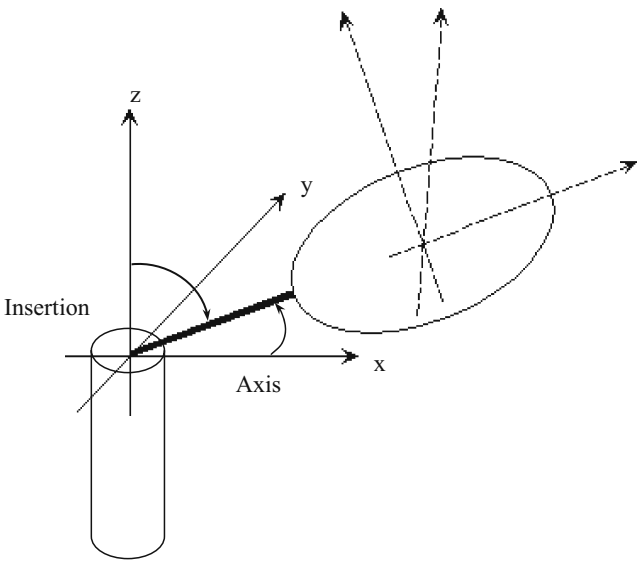

Fig. 4 Geometrical coordinate system of the architectural engine

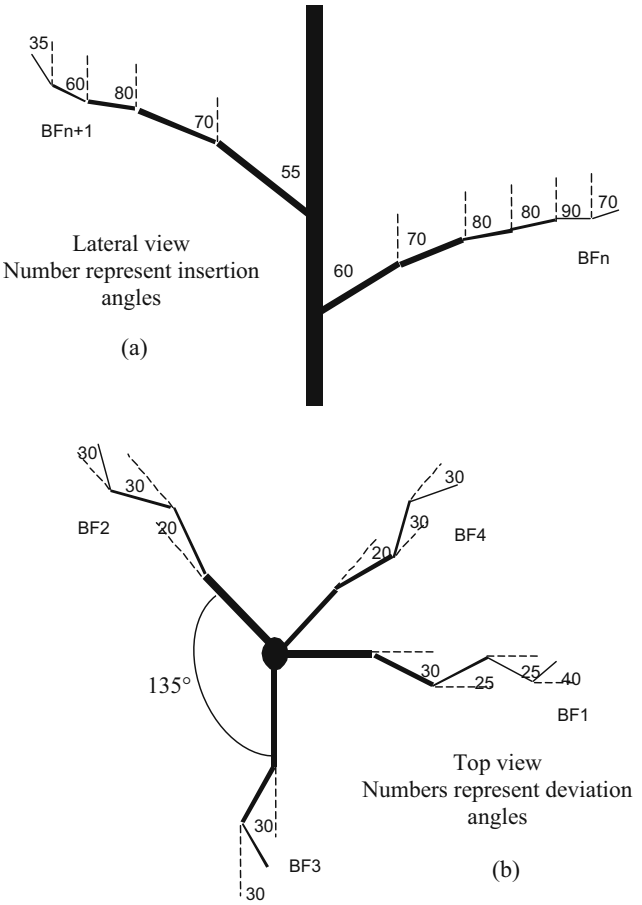

Fig. 5 Insertion angle and deviation angle on a cotton plant. **a** shows a lateral view of two consecutive fruiting branches, and **b** shows a top view with four fruiting branches

Thus, the parameters for the bending model are the insertion angle (θ_0), force (F), and its point of application (the insertion point of the last internode for each fruiting branch), the Young modulus (certainly variety dependent), and the diameter of the branch. We used a value of 1 for the force and 5 GPa for Young modulus. The component of morphology simulates the point of application and the diameter.

Fruiting branches do not have phyllotaxy. Our data (see Fig. 5b) show that axis angles for subsequent internode on a fruiting branch alternate and vary from 20° to 40°. We assume that these values are also variety dependent.

Fruit orientation is not really important, so we assume that squares and bolls are always oriented vertically, and we set their insertion angles to zero.

To simulate a virtual plant, with insertion angle, axes angle (both varietal parameters), and bending angle, we now need to know the length, diameter, and width of each organ and associate this organ with corresponding graphical symbols. This process is completed in the morphology component.

6.2 Organ Morphology

With the simulation of the actual growth of each organ, the system must be able to calculate "visual sizes." For leaves, petiole, peduncle, and fruit, "visual sizes" are based on weight estimations. Internode "visual sizes" are based on the age of the internode. For all the organs, the system calculates two values: length and width or angle. Angles are used for square and boll visualization because these symbols are composed of a number of subsymbols (e.g., five carpels for a boll) linked at their base but "free" at their top. Angles allow opening squares and boll as they grow.

Visualization values do not strictly represent reality (i.e., they do not follow a strict one-to-one relationship) because visual length and diameter of an organ are linked to the relative size of the adjoining other organ. Also, the actual capability of the two-dimensional graphical system of representation (there is no depth imaging in the current system) poses limitations which we have to respect given the intended target customer (an agricultural producer with access to traditional monitors and screens). For example, if we want to keep the same proportion between a mainstem and a peduncle, it will be impossible either to visualize all of the plant on the screen or to see the peduncles due to the limited screen resolution. Also, each organ is associated with a graphical image (a symbol, Fig. 3). These graphical symbols of organs are drawn independently without any consideration of scale (i.e., square and leaf drawing have the same size); thus, there is a size-scaling factor. The last organ graphical representation constraint is linked to the choice of representation of each organ. For example, a square has a graphical image approaching a pyramid in which the height is directly correlated with the size of the base. Then, in the case of a square, the system needs to know only the size of the base in order to represent a square of a certain weight. All these constraints lead to a representation that approaches visual reality but is certainly not equal to it. However, this representation is very close to reality, and the average human will not notice the divergence between the virtual organ and a true organ. Note that compromises to facilitate three-dimensional representations on a two-dimensional screen do not compromise the structural integrity of the plant's representation.

Figure 6 shows the relationship between boll dry weight and boll diameter. These relationships are different for the two cultivars tested. From the equations, we modeled the visual size of a boll with the generic equation:

$$\begin{aligned} \text{Size\_Boll} &= a + b \times \log \text{Weight\_Boll}, \\ &\quad \text{with Weight\_Boll} \leq c \\ \text{Angle\_Boll} &= d \times \text{Size\_Boll} \end{aligned} \tag{11}$$

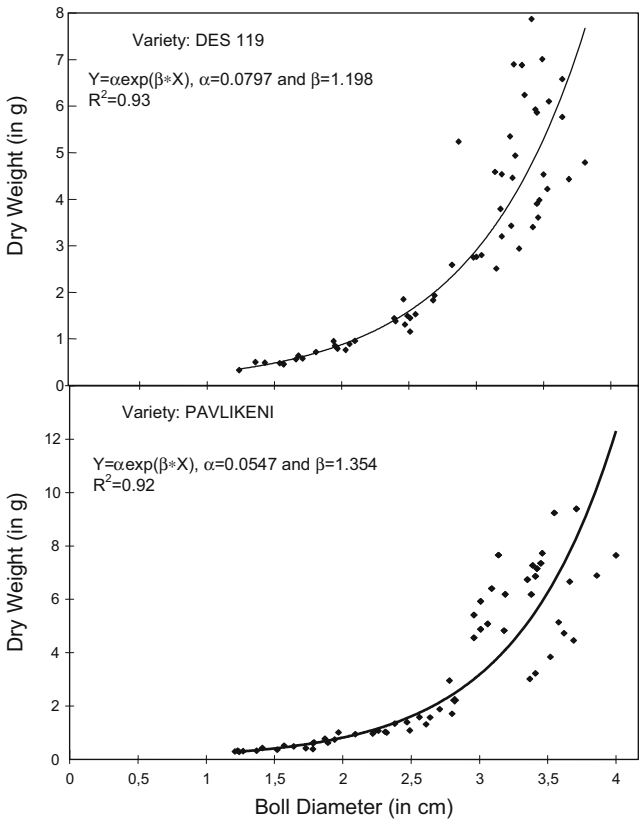

Fig. 6 Relation between the boll diameter and boll dry weight. Two different cultivars

where Weight_Boll is the boll dry weight in grams and a, b, and c three local variety-dependent parameters.

We did not have any data for squares because squares are very small and light so a relationship between weight and size would not be precise. Further, their presence or absence is significant but not their size. So, we decided to model the visual size of square with the following empirical generic equation:

$$\text{Size\_Square} = a + b \times \text{Weight\_Square}, \quad \text{with Weight\_Square} \leq c$$

$$\text{Angle\_Square} = d \times \text{Size\_Square}$$

where Weight_Square is the square dry weight in grams and a, b, and c three local variety-dependent parameters.

Leaf, petiole, and peduncle visual representations request also two information types: length and width or diameter. Figure 7 shows the relationship between leaf dry weight and leaf area for all the leaves collected on one plant, assuming a constant dry mass per unit length. Under the condition of our experiment, this relationship is independent of temperature treatment (the differences are

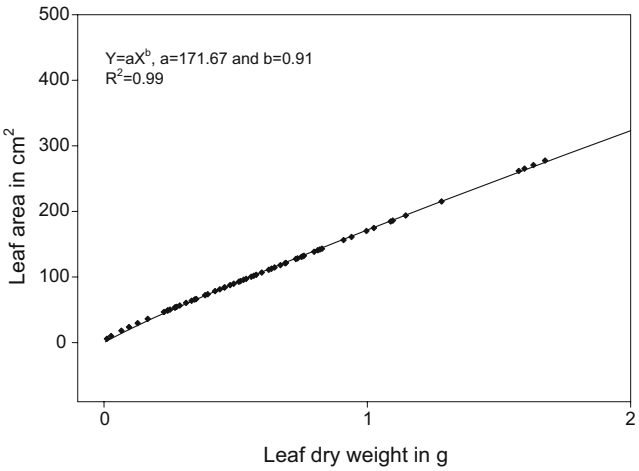

Fig. 7 Relationship between leaf dry weight and leaf area

not statistically significant, $P>0.05$). Leaf length and width can be expressed from leaf weight, and the equations are:

$$\text{Length\_Leaf} = a \times \text{Weight\_Leaf}^b \quad (13)$$

$$\text{Width\_Leaf} = c \times \text{Length\_Leaf}$$

where Weight_Leaf is the leaf dry weight in grams and a, b, and c three local variety-dependent parameters.

Figures 8 and 9 show the relationship between petiole dry weight and petiole length and between leaf dry weight and petiole dry weight, assuming a constant dry mass per unit length and a constant dry mass per unit area (value from [39]). By construction, these relations are also independent of temperature treatment. GOSSYM

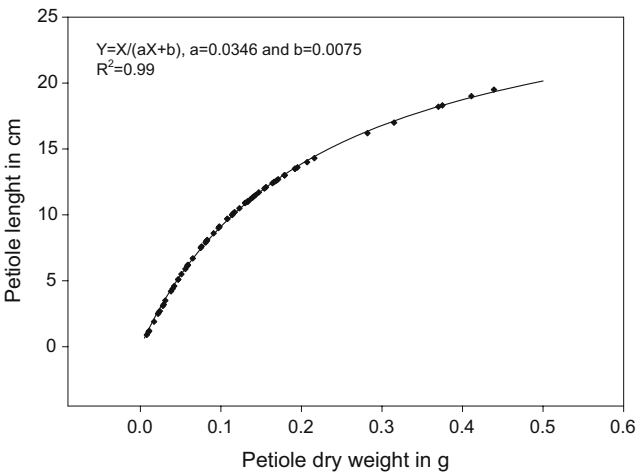

Fig. 8 Relationship between Petiole dry weight and petiole length

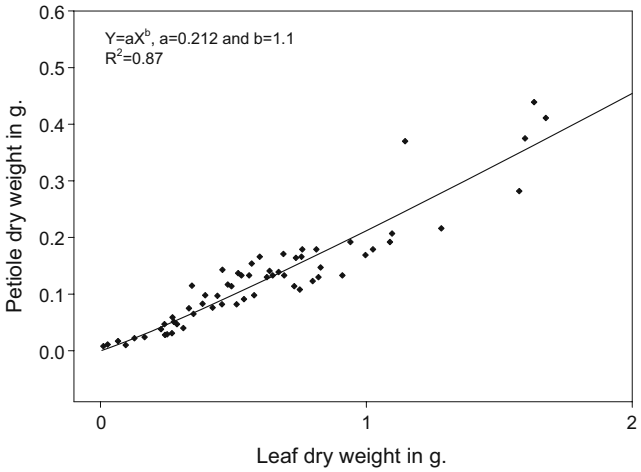

Fig. 9 Relationship between leaf dry weight and petiole dry weight

does not simulate explicitly petiole dry weight, but from our data, it is easy to infer it from leaf dry weight. The petiole equations are based from the leaf weight:

$$\text{Length\_Petiole} = \frac{a \times \text{Weight\_Leaf}^b}{c \times \text{Weight\_Leaf}^b + d} \quad (14)$$

$$\text{Diameter\_Petiole} = e \times \text{Length\_Petiole}$$

where Weight_Leaf is the leaf dry weight in grams and a, b, c, d, and e are five local variety-dependent parameters.

Figures 10 shows the peduncle length evolution in relation to the fruit age. The two groups of points (ca. before 10 days and after 20 days) indicate two different phases during peduncle growth. During the first period, fruit is at the square stage, and the peduncle stays short, then just after anthesis, the peduncle has a very fast length increase during a very short period. Because the length of the peduncle is negligible in comparison with other organ lengths, we did not model these two different phases. The peduncle equations are:

$$\text{Length\_Peduncle} = a \times \left(1 - e^{(-b \times \text{Age\_Organ})}\right) \quad (15)$$

$$\text{Diameter\_Peduncle} = c \times \text{Length\_Peduncle}$$

where Age_Organ is the age of the fruit in days and a, b, and c are three variety-dependent parameters.

7 Whole Plant and Plant Population Integration

Figures 11, 12, 13, and 14 show virtual plants simulated with the new system. The plant images can be rotated along the x-, y-, and z-axes and infinitely zoomed in or out. The figures shown represent average plants from a field. The simulation can be run continuously and stopped on any given day or allowed to proceed to simulate an entire season.

Figure 11 shows the simulation results for three different days (at 06/06, 08/04, and 10/13 for an emergence date at 5/13). The changes in size and organ distribution are a function of plant age and interactions with the environment. Note that the actual system shows a continuous "movie" of the plant as it grows, and only three images have been selected here for illustration.

Figure 11 corresponds to a simulation using high nitrogen and optimal water. Notice the complete maturation of the bolls, the abscission of most of the leaves, and a minor amount of regrowth (recall cotton is a perennial plant) beginning at the distal portion of the plant. Figure 12 corresponds to similar conditions than Fig. 11, but here nitrogen supply is 30% that of Fig. 11. Final fruit load is noticeably lower; a greater allocation has been made to vegetative development relative to reproductive set. This is due to the fact that more fruit was lost due to nitrogen stress. The system does not yet adjust colors to account for

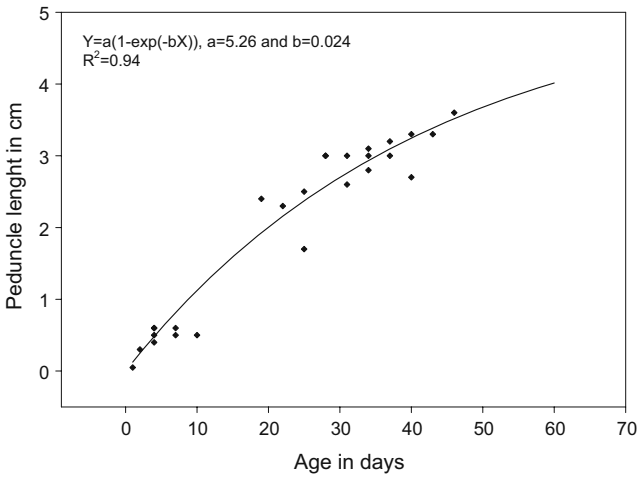

Fig. 10 Relationship between peduncle length and its age

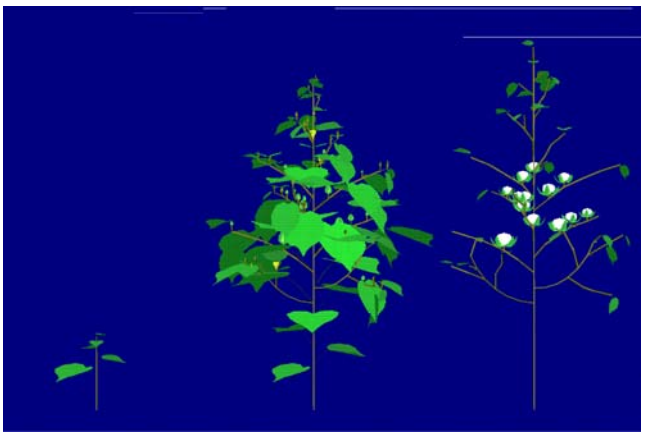

Fig. 11 Visualization at three different days of a plant average for a crop with high nitrogen fertilization and good water supply

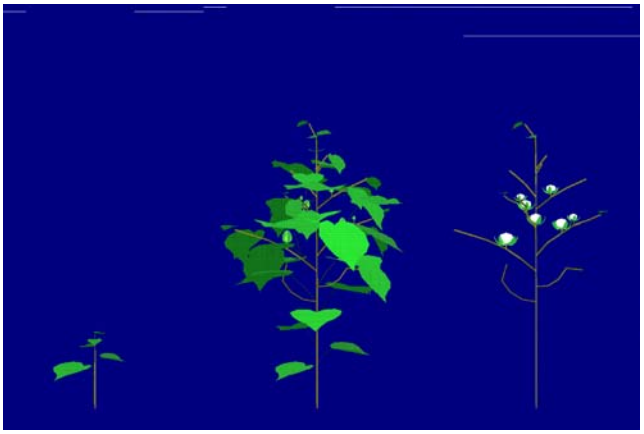

Fig. 12 Visualization at three different days of a plant average for a crop with low nitrogen fertilization and good water supply

the expected chlorosis and yellowing of the plant due to nitrogen or water stress. This enhancement will be made in the future and will represent a further significant departure from architectural-only models. Figure 13 corresponds to similar conditions than Fig. 11 and 12 but with no nitrogen and less water. The overall plant height is dramatically stunted, the number of leaves and fruit is greatly diminished, and it is obvious that this plant has been stressed and will produce a fraction of the yield of Fig. 11. Importantly, it can be seen that the distribution of yield is also dramatically different for all experiments. In cotton, quality is directly linked to fruit distribution and thus to final value of the yield. Figure 11 shows an optimal "bottom crop" (bolls produced low on the plant and close to the mainstem have the highest fiber quality). Figure 12 shows a shift to yield higher up on the mainstem, whereas Fig. 13 shows a "top crop" which in addition to lower yields will suffer from very low fiber quality. Figure 14 shows all three plants together at their final stage.

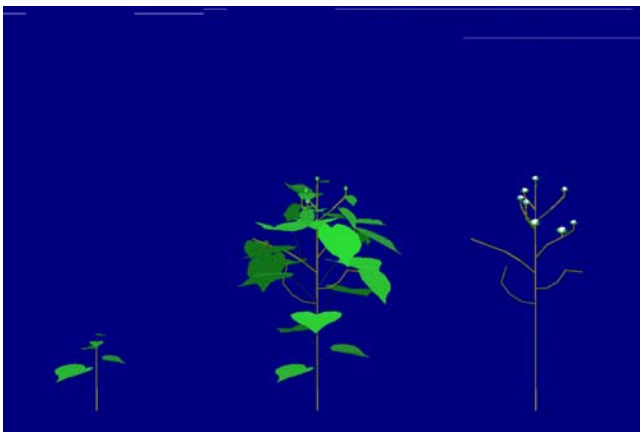

Fig. 13 Visualization at three different days of a plant average for a crop with no nitrogen fertilization and low water supply

8 Visualization, Topology, Architecture, and Functional Implications to the Modeling of Plants: Current Applications

Whereas traditional crop architectural models insisted on topology and architecture and mechanistic modeling insisted on physiological functionality, virtual crop models integrate both approaches. Because virtual plants can be manipulated and examined from any angle, features observable in the field can be also analyzed on the virtual plants [31]. Applications being implemented in the area of plant topology and visualization include the use of virtual crops for the study of population dynamics, optimal plant architectural forms, radiative phenomena, evapotranspiration, and the study of the implications of field variability.

A key feature of biological systems is the fact that they are variable (due to genetic and phenotypic expression). This variability is important for management because very dis-uniform fields will behave differently than more homogenous fields. With virtual representations, we can assess, compare, and understand the nature of this variability to better manage the system. Room et al. [34, 35] in Australia have developed a simple, L-system-based approach to the virtual representation of cotton plants. Earlier, de Reffye [11, 13, 15] in France developed probability-based virtual representations of cotton, coffee, and other plants. The applications being implemented by these researchers include the use of virtual crops for the study of population dynamics, optimal plant architectural forms, and the study of the implications of field variability to productivity. The present system lends itself similarly to such applications.

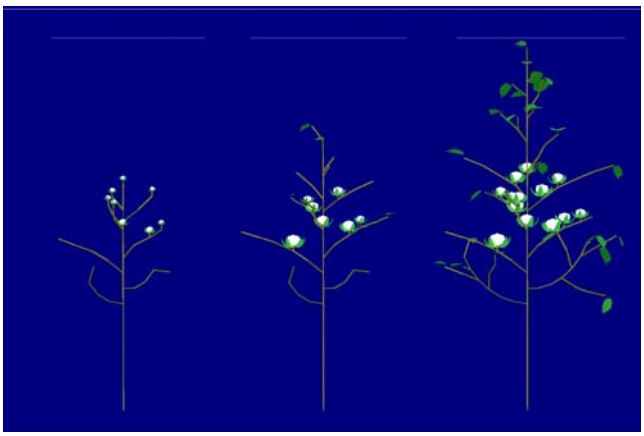

Fig. 14 Visualization of the three different plant averages at their final stage. Left plant represents a crop with no nitrogen and low water supply, middle plant represents a crop with low nitrogen supply but a good water supply and plant on the right represents a crop with optimal cultural inputs

Research applications of virtual cotton are important. For example, virtual cotton decision support systems will be an important extension of the possibilities for simulation models. A virtual plant can be tagged with light sensors and different plant architectures. Different models of photosynthesis can be tested to determine optimal plant forms. A researcher can initiate a simulation, apply stresses, and then measure intercepted light, growth characteristics, and other aspects before ever planting an actual seed. Different leaf shapes, plant spacing, weed competition, etc. can be similarly studied with a virtual tool. Another advantage is the direct correspondence between computer and real-world observations, which make the translation of observed to modeled phenomena and associated variability more straightforward. In addition to providing a direct surrogate for field experiments, the a priori knowledge gained from virtual experiments will make it easier for researchers to interact by examining the expected behavior before setting out research in the field [34]. The potential savings to funding and research institutions of these kinds of tools are enormous. Another application is in the area of sampling research. The availability of a virtual cotton field with virtual insects distributed in user-defined patterns will enable researchers to test many sampling schemes and prefilter algorithms prior to their field validation.

Virtual cotton can also be a decision-aid tool for producers. Virtual cotton fields will permit the modeling of heterogeneous areas analogous to real fields and will permit the inclusion/simulation of the genotypic/phenotypic variable expression of the crop. Plant maps, a key tool for model correction and record keeping, are more easily constructed using virtual representations than with two-dimensional abstractions. The visualization of the effects of different management practices on fruit distribution, for example, will be useful in selecting practices that minimize the adverse effects of a suboptimal fruit set and demonstrating clearly and convincingly the results of alternative practices.

Another important use of virtual plants resides in its use as training tools. One of the hurdles to overcome in introducing computer-based techniques to farmers is the learning curve associated with complex, management-oriented software. The use of virtual plants, of being able to traverse a virtual cotton field all the while making observations and recording data, will be an unparalleled tool for teaching optimal cultural practices and sampling and monitoring techniques. For example, in agricultural colleges, students will interactively see field effects of different management practices.

The objectives of this study were to improve the use of crop model as a decision support system but also as a training tool for everybody involved in agriculture production. The model resulting from our research allows a vastly improved model output interpretation and use of the model as a surrogate experimental environment, and it allows to better integrate our knowledge about how plants grow into a unique system.

9 Conclusions

This research integrates plant architectural modeling or "visualization modeling" and "mechanistic" or physiologically based modeling aiming to describe how a plant functions. The approach we developed was initially based on the "mechanistic" approach. The system was developed by enhancing a base "mechanistic" model, GOSSYM, with a three-dimensional architectural component. We accomplished this by associating to growth and development functions, actual locations in three-dimensional space. The proposed system presents the result of the simulation visually and through different reports. Visual capabilities make the proposed system very unique as it allows users to judge the results of the simulation the same way a farmer judges the situation of the crops in real life, by visually observing the field.

Finally, because of the high quality of visual outputs, the system can be used in faculty curriculums to teach future specialists the effects of agricultural practices on crop production using a virtual environment. Therefore, the model is freely available, and after request to the authors, anyone can download it from the ITK website (http://www.itkweb.com).

Appendix

The Bending Model

Generality

The elasticity of a material depends on the applied forces, the section of the material, and an intrinsic characteristic named Young's modulus [5]. For example, the elongation of a cylindrical bar can be expressed as:

$$h - h_0 = \frac{1}{E} \times \frac{h_0}{S} \times F \tag{16}$$

where: $h-h_0$ is the elongation, S the section, F the traction force applied at the end of the bar, and E the Young's modulus.

A fruiting branch can be assimilated to an embedded bar in the mainstem and submitted to a vertical force F (see below Fig. 15).

At the point of coordinates (x,y) by definition, the flexing moment M is:

$$M = E \times \mathrm{I} \times \frac{\mathrm{d}\theta}{\mathrm{d}S} \tag{17}$$

where: E is the Young module, I is the inertia ($\mathrm{I} = \frac{\pi R^4}{4}$ in the case of a bar with circular section, where R is the radius of the section), $\mathrm{d}S$ a small length of the bar, $\mathrm{d}\theta$ the angle between the tangent of two successive length portions of the bar, and $\frac{\mathrm{d}\theta}{\mathrm{d}S}$ the bending of the bar.

At the end of the bar where bending force is applied, the flexing moment is nil. At the point of (x, y) coordinates, the flexing moment M and the bending force equilibrate (see Fig. 15). This can be expressed as:

$$M = (e - y) \times F\cos\theta_0 + (h - x) \times F\sin\theta_0 \tag{18}$$

$$E \times \mathrm{I} \times \frac{\mathrm{d}\theta}{\mathrm{d}S} = (e - y) \times F\cos\theta_0 + (h - x) \times F\sin\theta_0 \tag{19}$$

where: $F\ \cos\theta_0$ is the "compression" component and $F\ \sin\theta_0$ is the "flexion" component.

By differentiation of Eq. 19 with respect to S, we obtain:

$$E \times I \times \frac{\mathrm{d}^2\theta}{\mathrm{d}S^2} = -F\cos\theta_0 \frac{\mathrm{d}y}{\mathrm{d}S} - F\sin\theta_0 \frac{\mathrm{d}x}{\mathrm{d}S} \tag{20}$$

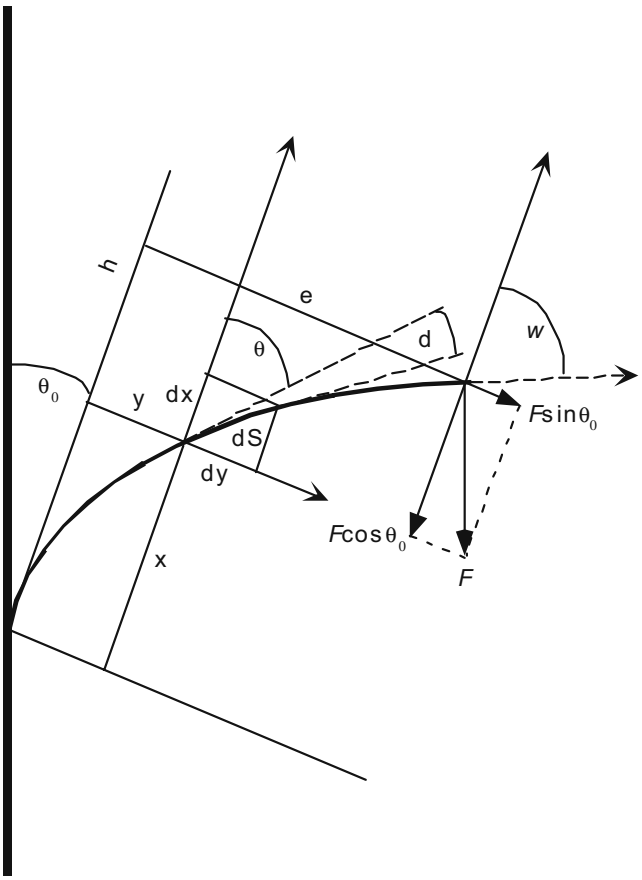

Fig. 15 Coordinate system used in the bending model

where: $\frac{\mathrm{d}y}{\mathrm{d}S} = \sin\theta$ and $\frac{\mathrm{d}x}{\mathrm{d}S} = \cos\theta$ (see Fig. 15) so Eq. 20 can be expressed as:

$$E \times \mathrm{I} \times \frac{\mathrm{d}^2\theta}{\mathrm{d}S^2} = -(F\cos\theta_0\sin\theta + F\sin\theta_0\cos\theta) \tag{21}$$

By multiplying Eq. 21 by $\frac{\mathrm{d}\theta}{\mathrm{d}S}$, we obtain:

$$E \times \mathrm{I} \times \frac{\mathrm{d}^2\theta}{\mathrm{d}S^2} \times \frac{\mathrm{d}\theta}{\mathrm{d}S} = -\left(F\cos\theta_0\sin\theta \times \frac{\mathrm{d}\theta}{\mathrm{d}S} + F\sin\theta_0\cos\theta \times \frac{\mathrm{d}\theta}{\mathrm{d}S}\right) \tag{22}$$

Then, by integration between w, the angle at the end of the bar, to θ with respect to S, because the flexion moment at the end of the bar is nil, we obtain:

$$\begin{aligned}\tfrac{1}{2} \times E \times I \times \left(\tfrac{\mathrm{d}\theta}{\mathrm{d}S}\right)^2 &= -F \times \left(\cos\theta_0[-\cos\theta]_w^\theta + \sin\theta_0[\sin\theta]_w^\theta\right) \\ &= F(\cos(\theta_0 + \theta) - \cos(\theta_0 + w))\end{aligned} \tag{23}$$

Then:

$$\begin{aligned}\mathrm{d}\theta &= \mathrm{d}S \times \sqrt{2\tfrac{F}{E \times I}(\cos(\theta_0 + \theta) - \cos(\theta_0 + w))} \\ &= K \times \sqrt{2} \times \sqrt{(\cos(\theta_0 + \theta) - \cos(\theta_0 + w))} \times \mathrm{d}S\end{aligned} \tag{24}$$

where: $\mathrm{K} = \sqrt{\frac{\mathrm{F}}{\mathrm{E} \times \mathrm{I}}}$

Case of small flexion

In the case of small flexion, w is small, θ is small too, and θ_0 varies from 0 to π. Equation 24 can be expressed as:

$$\mathrm{d}\theta = K \times \sqrt{2} \times \sqrt{A} \times \mathrm{d}S \tag{25}$$

where: $A = \cos(\theta_0 + \theta) - \cos(\theta_0 + w)$,

Because θ is small, we can approximate $\cos\theta$ by $\left(1 - \frac{\theta^2}{2}\right)$ (from Maclaurin's formula, n=2), $\cos w$ by $\left(1 - \frac{w^2}{2}\right)$, $\sin\theta$ *by* θ (from Maclaurin's formula, n=2), and $\sin w$ by w. Then, A can be expressed as:

$$\begin{aligned}A &= \left(1 - \tfrac{\theta^2}{2}\right) \times \cos\theta_0 - \theta\sin\theta_0 - \left(1 - \tfrac{w^2}{2}\right) \times \cos\theta_0 + w\sin\theta_0 \\ &= w \times \left(\sin\theta_0 + w\tfrac{\cos\theta_0}{2}\right) - (\sin\theta_0) \times \theta - \left(\tfrac{\cos\theta_0}{2}\right) \times \theta^2\end{aligned} \tag{26}$$

if: $a = w \times \left(\sin\theta_0 + w\frac{\cos\theta_0}{2}\right)$, $b = -(\sin\theta_0)$ and $\mathrm{c} = -\left(\frac{\cos\theta_0}{2}\right)$,
then: $A = a + b \times \theta + c \times \theta^2$. Equation 25 can be expressed as:

$$\mathrm{d}\theta = K \times \sqrt{2} \times \sqrt{a + b \times \theta + c \times \theta^2} \times \mathrm{d}S \tag{27}$$

We can express:

$$k + (\sin\theta_0) \times \theta + \left(\frac{\cos\theta_0}{2}\right) \times \theta^2 = \left(\alpha + \theta \times \sqrt{\frac{\cos\theta_0}{2}}\right)^2,$$

with:

$$2\alpha \times \sqrt{\frac{\cos\theta_0}{2}} = \sin\theta \quad \text{, or :} \quad \alpha = \frac{\sin\theta_0}{\sqrt{2\cos\theta_0}} \quad \text{and k} = \alpha^2.$$

Now, we have:

$$\left(\frac{\cos\theta_0}{2}\right) \times \theta^2 = \left(\theta \times \sqrt{\frac{\cos\theta_0}{2}} + \frac{\sin\theta_0}{\sqrt{2\cos\theta_0}}\right)^2 - \left(\frac{\sin\theta_0}{\sqrt{2\cos\theta_0}}\right)^2 - (\sin\theta_0) \times \theta$$

Replacing in Eq. 26, one obtains:

$$A = \left(w \times \sqrt{\frac{\cos\theta_0}{2}} + \frac{\sin\theta_0}{\sqrt{2\cos\theta_0}}\right)^2 - \left(\theta \times \sqrt{\frac{\cos\theta_0}{2}} + \frac{\sin\theta_0}{\sqrt{2\cos\theta_0}}\right)^2 \tag{28}$$

In the last expression, we can recognize that A is expressed in function of a constant a and a variable x. Then A is in the form of: $A = a^2 - x^2$, so Eq. 27 can be expressed as:

$$\mathrm{d}\theta = K \times \sqrt{2} \times \sqrt{a^2 - x^2} \times \mathrm{d}S, \tag{29}$$

where:

$$a = w \times \sqrt{\frac{\cos\theta_0}{2}} + \frac{\sin\theta_0}{\sqrt{2\cos\theta_0}}, \tag{30}$$

$$x = \theta \times \sqrt{\frac{\cos\theta_0}{2}} + \frac{\sin\theta_0}{\sqrt{2\cos\theta_0}} \tag{31}$$

In Eq. (31), x varies from $\frac{\sin\theta_0}{\sqrt{2\cos\theta_0}}$ to $w \times \sqrt{\frac{\sin\theta_0}{2}} + \frac{\sin\theta_0}{\sqrt{2\cos\theta_0}}$, because θ varies from 0 to w. By differentiation with respect to θ, Eq. 31 gives:

$$\mathrm{d}x = \sqrt{\frac{\cos\theta_0}{2}}\mathrm{d}\theta\mathrm{d}\theta = \frac{\mathrm{d}x}{\sqrt{\frac{cos\theta_0}{2}}}.$$

When replacing $\mathrm{d}\theta$ by $\mathrm{d}x$ in Eq. 27, we obtain:

$$\mathrm{d}x = \sqrt{\frac{\cos\theta_0}{2}} \times K \times \sqrt{2} \times \sqrt{a^2 - x^2} \times \mathrm{d}S, \quad \frac{dx}{\sqrt{a^2 - x^2}} = \sqrt{\cos\theta_0} \times K \times \mathrm{d}S \tag{32}$$

The length of the branch is h (see Fig. 15) so the integration with respect to S of Eq. 32 gives:

$$\int_{\frac{\sin\theta_0}{\sqrt{2\cos\theta_0}}}^{w\sqrt{\frac{\cos\theta_0}{2}}+\frac{\sin\theta_0}{\sqrt{2\cos\theta_0}}} \frac{\mathrm{d}x}{\sqrt{a^2 - x^2}} = \sqrt{\cos\theta_0} \times K \times h \tag{33}$$

By definition:

$$\int_{x1}^{x2} \frac{dx}{\sqrt{a^2 - x^2}} = \arcsin\frac{x2}{a} - \arcsin\frac{x1}{a} \quad \text{, and because}$$

$$a = w \times \sqrt{\frac{\cos\theta_0}{2}} + \frac{\sin\theta_0}{\sqrt{2\cos\theta_0}},$$

then, Eq. 33 can be expressed as:

$$\arcsin 1 - \arcsin\left(\frac{\frac{\sin\theta_0}{\sqrt{2\cos\theta_0}}}{w \times \sqrt{\frac{\cos\theta_0}{2}} + \frac{\sin\theta_0}{\sqrt{2\cos\theta_0}}}\right) = \sqrt{\cos\theta_0} \times K \times h \tag{34}$$

Solving for w gives:

$$w = \frac{\sin\theta_0\left(1 - \cos\left(\sqrt{\cos\theta_0} \times K \times h\right)\right)}{\cos\theta_0 \times \cos\left(\sqrt{\cos\theta_0} \times K \times h\right)} \tag{35}$$

References

1. Acock, B., Reddy, V. R., Hodges, H. F., Backer, D. N., & McKinion, J. M. (1985). Photosynthetic response of soybean canopies to full-season carbon dioxide enrichment. *Agronomy Journal 77*, 942–947.
2. Baker, D. N., Hesketh, J. D., et al. (1972). Simulation of growth and yield in cotton: I. Gross photosynthesis, respiration, and growth. *Crop Science*, *12*, 431–435.
3. Baker, D. N., & Landivar, J. A. (1990). The simulation of plant development in GOSSYM. In T. Hodges (Ed.), *Predicting crop phenology* (pp. 153–170). Boca Raton, FL: CRC.
4. Baker, D., McKinion, J. M., et al. (1983). GOSSYM: A simulator of cotton crop growth and yield. *South Carolina Agricultural Experiment Station Bulletin*, *1089*, 134.
5. Beer, F. P., & Johnson, E. R. J. (1981). *Mechanics of materials*. New York: McGraw-Hill.
6. Ben Porath, A. (1985). Effect of taproot restriction on growth and development of cotton grown under drip irrigation. Agronomy, Mississippi State, Mississippi State University, pp. 224.
7. Bouman, B. A. M., van Keulen, H., et al. (1996). The 'School of de Wit' crop growth simulation models: A pedigree and historical overview. *Agricultural Systems*, *52*(2/3), 171–198. doi:10.1016/0308-521X(96)00011-X.
8. Bruce, R. R., & Römkens, M. J. M. (1965). Fruiting and growth characteristics of cotton in relation to soil moisture tension. *Agronomy Journal*, *57*, 135–140.
9. Cox, P. G. (1996). Some issues in the design of agricultural decision support systems. *Agricultural Systems*, *52*(2/3), 355–381. doi:10.1016/0308-521X(96)00063-7.
10. de Reffye, P. (1976). Modélisation et simulation de de la verse du caféier, à l'aide de la théorie de la résistance des matériaux. *Cafe, Cacao, The*, *XX*(4), 251–271.
11. de Reffye, P. (1979). *Modélisation de l'architecture des arbres par des processus stochastistiques. Simulation spatiale des modèles tropicaux sous l'effet de la pesanteur. Application au coffea robusta*. Orsay, France: Paris-Sud. p. 195.

12. de Reffye, P. (1983). Modèle mathématique aléatoire et simulation de la croissance et de l'architecture de caféier Robusta. 4eme partie. Programmation sur micro-ordinateur du tracé en trois dimensions de l'architecture d'un arbre. Application au caféier. *Cafe, Cacao, The*, *XXVII*(1), 3–20.
13. de Reffye, P., Blaise, F., et al. (1993). Modélisation et simulation de l'architecture et de la croissance des plantes. *Revue*. *Palais de la Decouverte (Paris, France)*, *209*, 23–48.
14. de Reffye, P., & Duceau, P.(1977). Amélioration de la résistance à la verse du caféier à l'aide de la théorie de la résistance des matériaux. In *8ème Colloque Scientifique International sur le Café*, Abidjan, ASIC.
15. de Reffye, P., Edelin, C., et al. (1988). Plant models faithful to botanical structure and development. *Computers & Graphics*, *22* (4), 151–158. doi:10.1145/378456.378505.
16. de Wit, C. T., & Brouwer, R.(1968). Über ein dynamisches Modell des vegetativen Wachstums von Pflanzenbeständen. *Vereinigung für Angewandte Botanik* (Personal document).
17. Duncan, W. G., Loomis, R. S., et al. (1967). A model for simulating photosynthesis in plant communities. *Hilgardia*. *The Journal of Agricultural Science*, *38*, 181–205.
18. Egli, D. B. (1991). W.G. Duncan – father of crop models. *Journal of Agronomic Education*, *20*(2), 167–167 Fall.
19. Fisher, J. B., & Honda, H. (1979). Branch geometry and effective leaf area: A study of terminalia branching pattern. I. Theoretical Trees. *American Journal of Botany*, *66*, 633–644. doi:10.2307/2442408.
20. Fosner, R. (1997). *OpenGL. Programming for Windows 95 and Windows NT*. Redwood City, CA: Addison-Wesley.
21. Guinn, G. (1985). Fruiting of cotton. III. Nutritional stress and cutout. *Crop Science*, *25*, 981–985.
22. Hesketh, J. D., Baker, D. N., et al. (1972). Simulation of growth and yield in cotton. II. Environmental control of morphogenesis. *Crop Science*, *12*, 436–439.
23. Jallas, E. (1991). *Modélisation de Développement et de la Croissance du Cotonnier. Mémoire de DEA en Agronomie*. Paris: INA-PG, pp. 101.
24. Jallas, E. (1998). *Improved model-based decision support by modeling cotton variability and using evolutionary algorithms*. PhD dissertation in Biological Engineering, Mississippi State, Mississippi State University, pp. 239.
25. Kharche, S. D. (1984). Validation of GOSSYM: Effects of irrigation, leaf shape and plant population on canopy light interception, growth and yield of cotton. PhD dissertation in Agronomy, Mississippi State, Mississippi State University, pp. 173.
26. Lindenmayer, A. (1968). Mathematical models for cellular interaction in development, Parts I and II. *Journal of Theoretical Biology*, *18*, 280–315. doi:10.1016/0022-5193(68)90079-9.
27. Marani, A., Baker, D. N., et al. (1985). Effect of water stress on canopy senescence and carbone exchange rates in cotton. *Crop Science*, *25*, 798–802 September–October.
28. Papajorgji, P., & Pardalos, P. (2005). *Software engineering techniques applied to agricultural systems an object-oriented and UML approach*. New York: Springer.
29. Phene, C. J., Baker, D. N., et al. (1978). SPAR. A soil-plant–atmosphere-research system. *Transactions of the ASAE*, *21*, 924–930.
30. Philipeau, G. (1995). Théorie des Plans d'Expérince. ITCF, Paris France.
31. Prusinkiewicz, P., & Hammel, M. (1994). Visual models of morphogenesis. http://www.cpsc.ucalgary.ca/projects/bmv/vmm/animations.html.
32. Reddy, K. R., Reddy, V. R., & Hodges, H. F. (1992). Temperature effects on early season cotton growth and development. *Agronomy Journal*, *84*, 229–237.
33. Reddy, K. R., Hodges, H. F., & McKinion, J. M. (1993). Temperature effects on pima cotton leaf growth. *Agronomy Journal*, *85*, 681–686.
34. Room, P. M., Hanan, J. S., et al. (1996). Virtual plants: New perspectives for ecologists, pathologists and agricultural scientists. *Trends in Plant Science*, *1*(1), 33–38. doi:10.1016/S1360-1385(96)80021-5.
35. Room, P. M., Maillette, L., et al. (1994). Module and metamer dynamics and virtual plants. *Advances in Ecological Research*, *25*, 105–157. doi:10.1016/S0065-2504(08)60214-7.
36. Saugier, B., & Garcia de Cortazar, V. (1987). Modélisation de la croissance d'une culture, relation potentielle avec la sélection. *Le sélectionneur Français*, *39*, 7–18.
37. Sequeira, R. A., Olson, R. L., et al. (1996). An intelligent, interactive data input system for a cotton simulation system. *AI Application*, *10*(1), 41–56.
38. Sinko, J. W., & Streifer, W. (1967). A new model for age-size structure of a population. *Ecology*, *48*(6), 910–918. doi:10.2307/1934533.
39. Thanisawanyangkura, S., Sinoquet, H., et al. (1997). Leaf orientation and sunlit area distribution in cotton. *Agricultural and Forest Meteorology*, *86*, 1–15.